CRYSTAL GROWTH & DESIGN

pubs.acs.org/crystal

Article

Exploring the Crystal Structure Landscape of 3,5-Dinitrobenzoic Acid through Various Multicomponent Molecular Complexes

Matthew C. Scheepers and Andreas Lemmerer*

Cite This: https://dx.doi.org/10.1021/acs.cgd.0c01217

Read Online

ACCESS | Metrics & More | Article Recommendations | Supporting Information

ABSTRACT: Seven new multicomponent crystals, including one hydrate, one solvate, one molecular salt, and four cocrystals, consisting of 3,5-dinitrobenzoic acid with various coformers were synthesized and presented. These coformers include 2-acetylpyridine, 3-cyanopyridine, flufenamic acid, dimethylaminobenzophenone, pyridoxine, theophylline, and thiourea. Both hydrogen-bonding and weaker intermolecular forces such as C−H···π bonding, π-hole, and π···π contribute significantly to the overall packing scheme of each structure. Hirshfeld surfaces were used to identify these intermolecular forces. These structures were compared to those in the literature using the Cambridge Structural Database (CSD). These multicomponent crystals were characterized by single-crystal X-ray diffraction (SC-XRD) and differential scanning calorimetry (DSC).

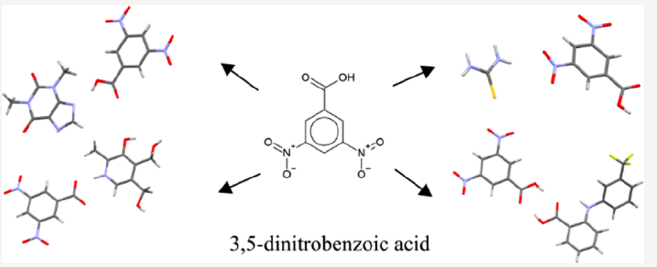

INTRODUCTION

The search for alternative methods for improving currently existing active pharmaceutical ingredients (APIs) with poor properties without modifying the drug itself has become critical. The formulation of APIs consisting of either a salt or a cocrystal has increased in the past few decades.[1−3] Cocrystals and molecular salts often have properties which differ significantly from those of the respective coformers. For pharmaceutical drugs improving properties such as solubility, tabletability, and intrinsic dissolution rates are critical, and the use of cocrystals has achieved this.[4,5] For this reason it makes the search for new multicomponent crystals so attractive.

3,5-Dinitrobenzoic acid (**dnba**), the molecule of interest in this work, consists of a carboxylic acid group and two nitro groups, all in a positions meta to each other. Several multicomponent crystal structures, both binary and ternary, involving **dnba** have been published in the Cambridge Structural Database (CSD),[6] including those which include various APIs.[7−9] A total of 278 results of cocrystals and molecular salts have been reported. Studies involving **dnba** include high energy density related materials,[10,11] short, strong hydrogen bonding[12] and the crystal engineering of APIs.[13−15] Although the primary interactions will be due to the formation of a hydrogen bond between the carboxylic acid and a suitable hydrogen bond acceptor of the coformer, other types of weaker interactions exist and could contribute significantly. For example, π holes from the nitro groups can form directional intermolecular interactions between neighboring molecules.[16] Due to the strongly electron withdrawing nitro groups the ring of **dnba** is relatively π-electron poor, which therefore makes **dnba** a potential charge-transfer acceptor molecule.

In this work we present seven new multicomponent crystals of **dnba**, which formed one solvate, one hydrate, one molecular salt, and four cocrystals. Most of the coformers chosen consist of N-containing heterocycles, with the rest consisting of various functional groups. These coformers include 2-acetylpyridine (**2acp**), 3-cyanopyridine (**3cnp**), flufenamic acid (**fa**), dimethylaminobenzophenone (**dmabp**), pyridoxine (**pyd**), theophylline (**thp**), and thiourea (**tu**) (see Scheme 1). Two of these coformers are APIs: **fa** is a nonsteroidal anti-inflammatory (NSAID) drug, while **thp** is used as a muscle relaxant or vasodilator in the treatment of respiratory issues such as asthma.[17,18] **pyd**, also referred to as vitamin B_6, is a nitrogen-containing heterocycle with several hydroxyl groups which can form potential hydrogen bonds with the nitro groups of **dnba**. **3cnp** and **2acp** were chosen to explore more crystal forms of these compounds as well, since not many crystal structures involving these compounds have been reported. **dmabp**, a derivative of benzophenone, is generally used as a photoinhibitor.[19] **dmabp** is structurally similar to Michler's ketone, which is used as an intermediate in the synthesis of various dyes. Although various benzophenone derivatives have been explored as potential coformers with **dnba**, only **dmabp** formed a multicomponent crystal. The aim

Received: September 1, 2020
Revised: December 3, 2020

Scheme 1. Structures of dnba and the Coformers Used for This Work

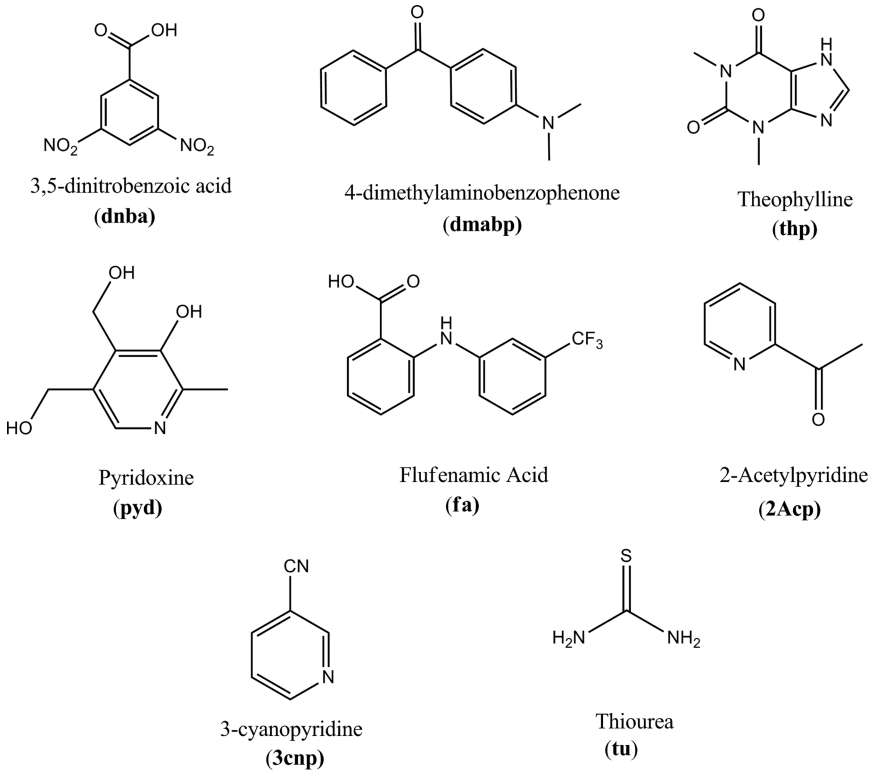

Table 1. Solvent System Used to Synthesize the Respective Multicomponent Molecular Complex

coformer	mass used (g)	solvent system
2-acetylpyridine	1.08 (1 mL, 8.915 mmol)	ethanol
3-cyanopyridine	0.049 (0.471 mmol)	ethanol
diethylaminobenzophenone	0.106 (0.471 mmol)	methanol[a]
flufenamic acid	0.133 (0.471 mmol)	ethanol/water (1/1 v/v)/ acetic acid
pyridoxine	0.080 (0.471 mmol)	ethanol
theophylline monohydrate	0.093 (0.471 mmol)	ethyl acetate
thiourea	0.036 (0.471 mmol)	ethyl acetate
3-aminopyridine	0.049 (0.471 mmol)	ethanol

[a]It should be noted that trace amounts of water were present in the starting material for methanol. This, along with the possibility of water from the atmosphere, resulted in the formation of the hydrate.

of this work is to observe new supramolecular assemblies with **dnba**, using a diverse range of coformers.

EXPERIMENTAL SECTION

All reagents used for synthesis and characterization were of analytical grade and were purchased from Sigma-Aldrich. Reagents were used as received, without further purification. Equimolar amounts of **dnba** (100 mg, 0.471 mmol) and the respective coformers were stirred in a heated solution of the respective solvent until no solid remained. This solution was left loosely covered, which evaporated to yield the respective cocrystal/salt. See Table 1 for the solvent systems used.

It should be noted that although several different solvents were used in an attempt to obtain a multicomponent crystal in a relatively high yield and pure form, those solvents did not yield the desired multicomponent crystal. In addition, several molar ratios were used (e.g. 2:1, 1:2, etc. **dnba**:coformer), but this yielded a mixture of the desired multicomponent crystal (in a 1:1 ratio) with the excess component. Heating was found to be essential in most of the cases (the multicomponent crystals consisting of the pyridine-based coformers did not essentially need heating, although heating helped in acquiring complete dissolution quickly), otherwise the desired multicomponent crystal could not be obtained.

Powder X-ray Diffraction (PXRD). Powder X-ray diffraction data for all compounds were measured at 293 K on a Bruker D2 Phaser diffractometer which employed a sealed-tube Co X-ray source (λ = 1.78896 Å), operating at 30 kV and 10 mA, and a LynxEye PSD detector in Bragg–Brentano geometry. Powder patterns for each sample are given in the Supporting Information, where the experimentally obtained data are compared to the calculated patterns obtained from the SC-XRD data.

Single Crystal X-ray Diffraction (SC-XRD). A Bruker D8 VENTURE PHOTON CMOS 100 area detector diffractometer, equipped with a graphite-monochromated Mo Kα_1 sealed tube (50 kV, 30 mA), was used to collect all of the intensity data. Crystal structures were determined at 173 K to achieve satisfactory thermal ellipsoids. The program SAINT+, version 6.02,[20] was used to integrate the data, and the program SADABS[21] was used to make empirical absorption corrections. Space group assignments were made using XPREP[21] on all compounds. In all cases, the structures were solved in the WinGX Suite of programs[21] by direct methods using SHELXS-97[21] and refined using full-matrix least-squares/difference Fourier techniques on F^2 using SHELXL-97.[21] All non-hydrogen atoms were refined anisotropically. All carbon-bound hydrogen atoms were placed at idealized positions and refined as riding atoms with its

https://dx.doi.org/10.1021/acs.cgd.0c01217
Cryst. Growth Des. XXXX, XXX, XXX−XXX

U_{iso} parameter being 1.2 or 1.5 times those of their parent atoms. Unless otherwise stated, nitrogen-bound and oxygen-bound hydrogen atoms were located in the difference Fourier map and their coordinates and isotropic displacement parameters refined freely. Diagrams and publication material were generated using ORTEP-3[22] and Mercury.[23]

Cambridge Structural Database Analysis. The Cambridge Structural Database (CSD)[6] was analyzed to determine any common trends occurring among different multicomponent structures consisting of **dnba**. A combined query using both the carboxylic acid form of **dnba** and the carboxylate form was used to search for entries. Entries were filtered using 3D coordinates and organics. Entries containing salts with alkali or alkali-earth cations, heavily disordered molecules, and/or solvates were not examined. Mercury[23] was used to inspect the crystal structures.

Crystal structures were determined to be binary, ternary, or greater and consist of either or both the protonated (carboxylic acid form) and deprotonated (carboxylate) forms. In the case of a ternary or greater structure, only the interactions involving **dnba** were considered. In the case of multiple entries of the same crystal structure, only one entry was inspected and counted.

Hirshfeld Surface Analysis. Hirshfeld surface analysis is a computational method that can be used to explore intermolecular interactions in molecular crystals that are weaker than hydrogen bonds,[24−26] as well as to determine the "shape" of molecular fragments, which are key to understanding the overall packing. The figures and fingerprint plots presented in this work were generated using Crystal Explorer 17.5.[27] All images were generated using a high (standard) resolution.

Differential Scanning Calorimetry (DSC). Differential scanning calorimetry data were collected using a Mettler Toledo 822^e instrument with aluminum pans under nitrogen gas (flow rate 10 mL/min). Exothermic events were shown as peaks. Samples were heated and cooled to determine melting points as well as any additional phase transitions. The temperature and energy calibrations were performed using pure indium (purity 99.99%, mp 156.6 °C, heat of fusion 28.45 J g^{-1}) and pure zinc (purity 99.99%, mp 479.5 °C, heat of fusion 107.5 J g^{-1}).

RESULTS AND DISCUSSION

Seven multicomponent crystals containing **dnba** have been synthesized, of which four are cocrystals, one is a hydrate, one is a solvate, and one is a salt. It should be noted that for the pyridine derivatives and theophylline it is possible for either a salt or a cocrystal to form. A "rule of thumb" exists that if the pK_a values of both compounds are known, it is possible to predict whether a salt or cocrystal will form. This is done by calculating the ΔpK_a, which is given by the formula,

$$\Delta pK_a = pK_a(\text{conjugate acid of base}) - pK_a(\text{acid})$$

If the ΔpK_a value is less than zero a cocrystal would form (if it forms), whereas a value greater than 2−3 should lead to a salt. Values between 0 and 3 can predict neither case and are 0 for the crystal systems in question.[27] For this work, **dnba** could have formed either a salt or a cocrystal with **2acp**, **3cnp**, **pyd**, **thp** and **tu**. Table 2 gives the comparison of the results predicted by the pK_a rule vs the actual results of the crystal structures formed. It shows that the rule works for at least three of the five multicomponent crystal structures.

Table 2. Comparison of the Result Predicted by the pK_a Rule vs the Actual Result of the Crystal Structures Formed[a]

coformer	pK_a of coformer	ΔpK_a	result based on rule	actual result
2acp	3.00	0.33	undetermined	cocrystal
3cnp	1.78	0.23	undetermined	cocrystal
Pyd	9.63	6.86	salt	salt
thp	8.60	5.83	salt	cocrystal
tu	1.44	−1.33	cocrystal	cocrystal

[a] pK_a for **dnba** = 2.77. Values from SciFinder.[28]

These crystals were characterized, and a description of each crystal structure is given below (Figure 1). Crystallographic data and hydrogen bonds are given in Tables 3 and 4, respectively. Hirshfeld surfaces for d_i, d_e, d_{norm}, the shape index, and curvedness and the respective fingerprint plots were generated and are presented in the Supporting Information unless stated otherwise. The discussion of each of the Hirshfeld surfaces generated for each molecular complex are discussed together with the description of the crystal structures.

Crystal Structure Descriptions of Dnba Complexes. ***dnba* + *2acp*.** **dnba** formed a solvate with **2acp**, forming colorless plates (Figure 2). The solvate crystallizes in the $P2_1/n$ space group, with the asymmetric unit consisting of one molecule each of **dnba** and **2acp**. **dnba** forms a discrete hydrogen bond to the pyridinium of **2acp** with the carboxylic acid group. This dimer forms 2D sheets which stack together.

The Hirshfeld surfaces generated revealed additional intermolecular interactions present in the crystal. Red spots on the d_{norm} surface indicate the presence of weak C−H···O hydrogen bond interactions, with both the acetyl and nitro groups being involved. The shape index shows that N−O···π and C−O···π formed from the nitro and acetyl groups, respectively. The shape index does not indicate the presence of any π···π type interactions, which is normally indicated by the presence of a red and blue triangle touching each other. These surfaces correlate well with the observed overall packing pattern of the crystal: the weak C−H···O hydrogen bonds favor the formation of different "layers", while the N−O···π and C−O···π interactions allows the "layers" to stack together.

***dnba* + *3cnp*.** **dnba** formed a cocrystal with **3cnp**, forming colorless needles (Figure 3). The cocrystal crystallizes in the $P2_1/c$ space group, with the asymmetric unit consisting of one molecule each of **dnba** and **3cnp**. **dnba** forms a discrete hydrogen bond to the pyridine of **3cnp** with the carboxylic acid group. The **3cnp** and **dnba** molecules form alternating columns of each molecule which then stack together with inversion of molecules along its column.

The Hirshfeld surface revealed additional interactions. From the d_{norm} red spots occurring at the cyano nitrogen (N4) and one of the aromatic hydrogens (H10) indicates the formation of a 3-cyanopyridine dimer, with a the graph set $R_2^2(10)$. Large red spots near the nitro groups are indicative of π-hole type interactions. Two cases exist: one where the partially positive π system of the ring of **dnba** interacts with the oxygen of a nitro group that is on a neighboring **dnba** and the other case one of oxygen of the carboxylic acid interacting with the nitrogen of the nitro group of a neighboring **dnba** molecule. Smaller red spots on the d_{norm} indicate the presence of C−H···π type interactions. As a result of the presence of the π-hole-type interactions, the shape index consists of various large "bumps" and "hollows", as indicated by regions of large blue and red spots, respectively, giving rise to various small regions of "flatness", as indicated by the curvedness. As a result, the columns of **dnba** and **3cnp** are held together by π-hole and weak C−H···N interactions, respectively, while the strong hydrogen bond between **dnba** and **3cnp** as well as a few C−

https://dx.doi.org/10.1021/acs.cgd.0c01217
Cryst. Growth Des. XXXX, XXX, XXX−XXX

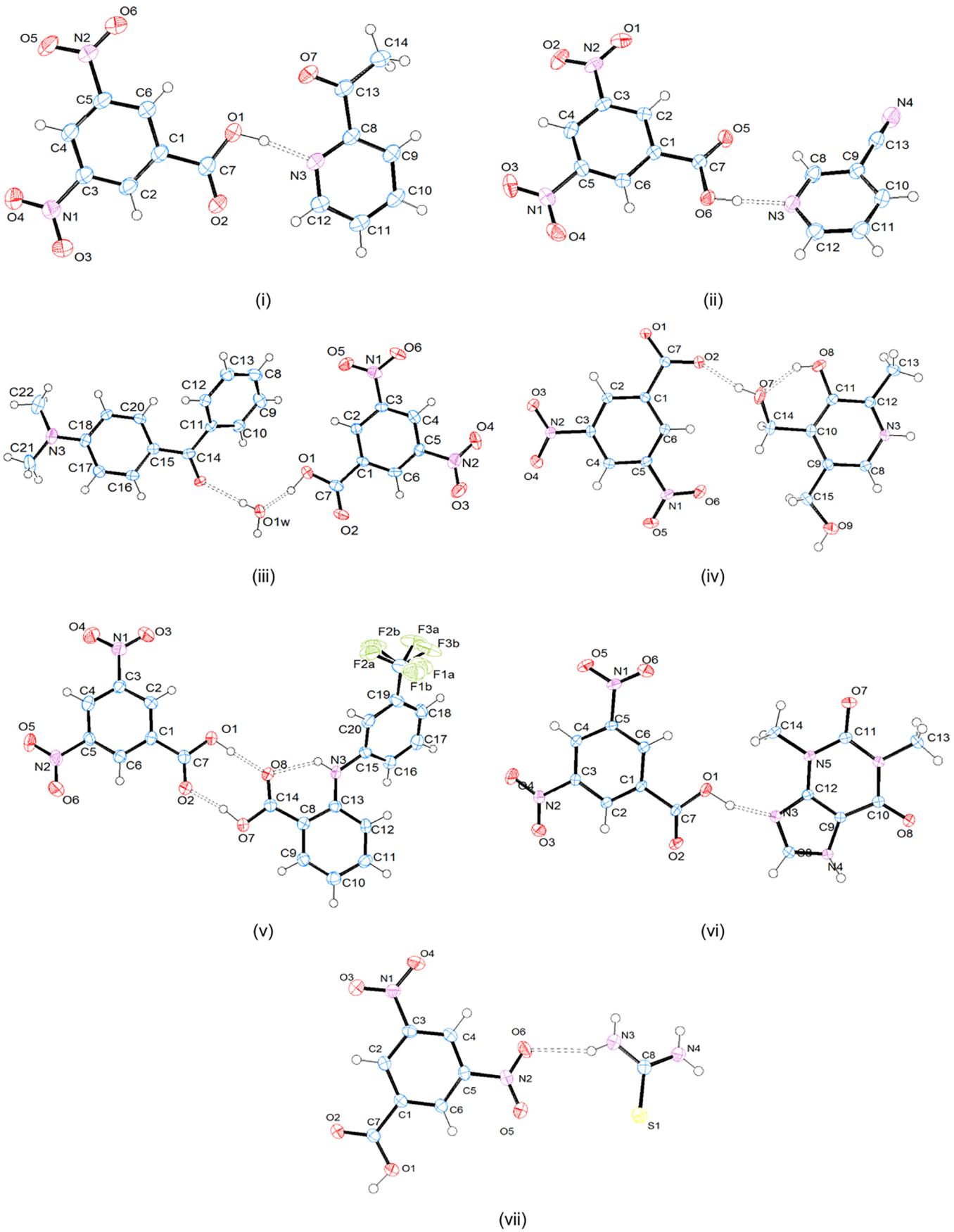

Figure 1. Ortep diagrams for the asymmetric units for the crystal structures of (i) **dnba** + **2acp**, (ii) **dnba** +**3cnp**, (iii) **dnba** + **dmabp**, (iv) **dnba** + **pyd**, (v) **dnba** + **fa**, (vi) **dnba** + **thp**, and (vii) **dnba** + **tu**, which shows the atom-numbering scheme. Displacement ellipsoids are drawn at the 50% probability level, and H atoms are shown as small spheres of arbitrary radii. The symmetry-independent hydrogen bonds are shown as dashed lines.

https://dx.doi.org/10.1021/acs.cgd.0c01217
Cryst. Growth Des. XXXX, XXX, XXX−XXX

Table 3. Summary of Crystallographic Data

	cocrystal + salt			
	dnba + 2acp	**dnba + 3cnp**	**dnba + dmabp**	**dnba + fa**
empirical formula	$C_{14}H_{11}N_3O_7$	$C_{13}H_8N_4O_6$	$C_{22}H_{21}N_3O_8$	$C_{21}H_{14}N_3O_8F_3$
formula wt	333.26	316.23	455.42	493.35
temp (K)	173(2)	173(2)	173(2)	173(2)
cryst syst	monoclinic	monoclinic	monoclinic	triclinic
space group	$P2_1/n$	$P2_1/c$	$P2_1/n$	$P\bar{1}$
a (Å)	8.9295(9)	6.1678(3)	10.0968(2)	7.6667(4)
b (Å)	13.9281(14)	9.2276(5)	21.2232(5)	10.7718(5)
c (Å)	11.8082(11)	24.0942(13)	10.3367(3)	13.4392(5)
α (deg)	90	90	90	70.846(2)
β (deg)	100.347(3)	96.703(2)	101.2240(10)	84.228(2)
γ (deg)	90	90	90	88.073(2)
V (Å^3)	1444.7(2)	1361.92(12)	2172.65(9)	1043.11(8)
Z	4	4	4	2
density (g/cm^3)	1.532	1.542	1.392	1.571
μ (mm^{-1})	0.126	0.126	0.108	0.139
F(000)	688	648	952	504
crystal size (mm^3)	0.512 × 0.248 × 0.248	0.347 × 0.258 × 0.159	0.213 × 0.221 × 0.268	0.142 × 0.117 × 0.052
2θ range for data collection (deg)	4.566−56.922	6.652−55.984	1.919−28.335	3.222−50.998
no. of rflns collected	13893	27504	41576	15916
no. of indep rflns	3638 (R(int) = 0.0717, $R(\sigma)$ = 0.0614)	3286 (R(int) = 0.0451, $R(\sigma)$ = 0.0289)	2901 (R(int) = 0.0953, $R(\sigma)$ = 0.0361)	3871 (R(int) = 0.0746, $R(\sigma)$ = 0.0776)
goodness of fit on F^2	1.022	1.037	1.015	1.098
final R indexes ($I \geq 2\sigma(I)$)	R1 = 0.0553, wR2 = 0.1420	R1 = 0.0473, wR2 = 0.1032	R1 = 0.0458, wR2 = 0.0944	R1 = 0.0660, wR2 = 0.1413
final R indexes (all data)	R1 = 0.0936, wR2 = 0.1678	R1 = 0.0679, wR2 = 0.1124	R1 = = 0.0759, wR2 = 0.1037	R1 = 0.1308, wR2 = 0.1636
CCDC	2026651	2026652	2026653	2026654

	cocrystal/salt		
	dnba + pyd	**dnba + thp**	**dnba + tu**
empirical formula	$C_{15}H_{15}N_3O_9$	$C_{14}H_{12}N_6O_8$	$C_8H_8N_4O_6S$
formula wt	381.3	392.3	288.24
temp (K)	173(2)	173(2)	173(2)
cryst syst	monoclinic	monoclinic	monoclinic
space group	$P2_1/n$	$C2/c$	$P2_1/c$
a (Å)	9.2152(5)	18.7625(6)	13.0957(2)
b (Å)	14.1356(7)	15.4699(6)	9.0162(2)
c (Å)	12.5534(6)	12.6823(4)	9.8594(2)
α (deg)	90	90	90
β (deg)	104.378(2)	117.917(2)	92.6450(10)
γ (deg)	90	90	90
V (Å^3)	1584.02(14)	3252.7(2)	1162.89(4)
Z	4	8	4
density (g/cm^3)	1.599	1.602	1.646
μ (mm^{-1})	0.135	0.134	0.31
F(000)	792	1616	592
crystal size (mm^3)	0.215 × 0.436 × 0.080	0.415 × 0.401 × 0.206	0.243 × 0.193 × 0.163
2θ range for data collection (deg)	6.296−55.984	5.266−55.998	3.114−55.994
no. of rflns collected	36275	36969	17130
no. of indep rflns	3814 (R(int) = 0.0344, $R(\sigma)$ = 0.0172)	3044 (R(int) = 0.0357, $R(\sigma)$ = 0.0219)	2797 (R(int) = 0.0506, $R(\sigma)$ = 0.0393)
goodness of fit on F^2	1.061	1.061	1.014
final R indexes ($I \geq 2\sigma(I)$)	R1 = 0.0405, wR2 = 0.1108	R1 = 0.0427, wR2 = 0.1186	R1 = 0.0368, wR2 = 0.0819
final R indexes (all data)	R1 = 0.0521, wR2 = 0.1227	R1 = 0.0501, wR2 = 0.1247	R1 = 0.0616, wR2 = 0.0933
CCDC	2026655	2026656	2026657

H···π interactions allow the columns to alternate with each other, as observed in the overall packing.

***dnba* + *pyd*.** **dnba** and **pyd** formed molecular salts, which crystallized as yellow prismatic crystals (Figure 4). The asymmetric unit consists of one molecule each of **dnba** and **pyd**, which crystallized in the $P2_1/n$ space group. A proton transfer occurred between the carboxylic acid of **dnba** and the pyridinium of **pyd**. One of the hydroxyl groups forms an intramolecular hydrogen bond with another neighboring hydroxyl group (O8−H8···O7). **dnba** and **pyd** form several different hydrogen bonds that form a continuous 2D lattice, with these lattices stacking on top of each other.

https://dx.doi.org/10.1021/acs.cgd.0c01217
Cryst. Growth Des. XXXX, XXX, XXX−XXX

Table 4. Hydrogen Bonds

D−H···A	d(D−H) (Å)	d(H···A) (Å)	d(D···A) (Å)	∠(DHA) (deg)
dnba + 2acp				
O1−H1···N3	0.98(3)	1.73(3)	2.707(2)	171(3)
dnba + 3cnp				
O6−H6···N3	0.93(2)	1.74(3)	2.6684(19)	175(2)
dnba + dmabp				
O1W−H1WA···O7[a]	0.92(6)	1.93(6)	2.842(5)	170(5)
O1W−H1WB···O7	0.77(6)	2.02(6)	2.789(5)	180(6)
O1−H2A···O1W	1.01(7)	1.57(6)	2.558(4)	164(6)
dnba + fa				
O1−H1···O8	0.92(5)	1.72(5)	2.625(4)	167(5)
N3−H3···O1[b]	0.98(2)	1.65(2)	2.6269(15)	174(2)
N3−H3···O2[b]	0.98(2)	2.57(2)	3.2529(15)	126(2)
O9−H9···O4[c]	0.88(3)	2.15(3)	3.0239(17)	175(2)
O7−H7···O2	0.87(3)	1.76(3)	2.6019(15)	162(2)
O8−H8···O7	0.86(3)	1.80(3)	2.5685(17)	147(3)
dnba + thp				
N4−H4···O8[d]	0.98(3)	1.76(3)	2.7264(16)	172(2)
O1−H1···N3	1.01(3)	1.66(3)	2.6264(15)	160(3)
dnba + pyd				
N3−H3···O1[h]	0.98(2)	1.65(2)	2.6269(15)	174(2)
N3−H3···O2[h]	0.98(2)	2.57(2)	3.2529(15)	126(2)
O9−H9···O4[c]	0.88(3)	2.15(3)	3.0239(17)	175(2)
O7−H7···O2	0.87(3)	1.76(3)	2.6019(15)	162(2)
O8−H8···O7	0.86(3)	1.80(3)	2.5685(17)	147(3)
dnba + tu				
N4−H4B···S1[e]	0.89(2)	2.49(2)	3.3773(18)	173(2)
N3−H3A···O6	0.82(2)	2.39(2)	3.108(2)	146(2)
N4−H4A···S1[f]	0.85(2)	2.66(2)	3.4502(19)	157(2)
N3−H3B···S1[f]	0.89(2)	2.66(3)	3.470(2)	152(2)
O1−H1···O2[g]	0.88(3)	1.77(3)	2.6524(18)	176(3)
N4−H4B···S1[e]	0.89(2)	2.49(2)	3.3773(18)	173(2)

[a] $-x+1, -y+1, -z+2$. [b] $x-1/2, -y+1/2, z+1/2$. [c] $x-1/2, -y+3/2, z+1/2$. [d] $-x+3/2, -y+3/2, -z+1$. [e] $-x+1, -y+1, -z$. [f] $-x+1, y+1/2, -z+1/2$. [g] $-x+2, -y, -z+2$. [h] $x-1/2, -y+1/2, z+1/2$.

The Hirshfeld surfaces for the molecular salt of **dnba + pyd** show that the hydrogen bond is the most significant intermolecular interaction present. The large, bright red spots present in the d_{norm} are involved with hydrogen bonding, with a few smaller and dimmer set of red spots which are involved with weaker C−H···O hydrogen bonding. Although the shape index has the presence of red and blue triangles that are typical indicators for the presence of a $\pi\cdots\pi$ interaction, the blue edges on the curvedness surface indicate otherwise. Most likely the 2D lattices formed are stacked together by a combination of both ionic forces and weak C−H···O interactions.

dnba + dmbp Hydrate. **dnba** and **dmabp** formed a hydrated molecular complex and crystallized as fragile orange plates (Figure 5). This molecular complex crystallized in the $P2_1/n$ space group with the asymmetric unit consisting of one molecule of each **dnba**, **dmabp**, and water. **dnba**, **dmabp**, and water form part of a dimer, where water acts as the primary hydrogen bond donor and acceptor. In this structure, water forms a bridge between **dnba** and **dmabp** by acting as a hydrogen bond acceptor from **dnba** and as a hydrogen bond donor to **dmabp** and another water molecule. These dimers formed 2D sheets which stack to form a layered structure.

The Hirshfeld surface reveals the presence of both π-hole and $\pi-\pi$ stacking in addition to the hydrogen bonding present. The bright red spots observed on the d_{norm} surface are related to the previously described strong hydrogen bonding. A few red spots appear over the nitro group O5−N1−O6 which indicates the presence of a π-hole-type interaction to the carboxylic acid group of an adjacent **dnba** molecule. The shape index indicates the presence of several $\pi-\pi$ stacking type interactions due to the presence of adjacent red and blue triangles on the surface. The first of these is between adjacent benzene rings (C8−C13) of **dmabp**, while the second of these is between the rings of **dnba** and the ring containing the dimethylamino group of **dmabp** (C15−C20). The curvedness shows regions which would allow for the possibility of $\pi-\pi$ stacking. This indicates that while hydrogen bonding yields the formation of the 2D sheets, these sheets are held together via π-hole and $\pi-\pi$ stacking interactions.

dnba + fa. **dnba** formed a cocrystal with **fa**, which crystallized as fragile, orange platelike crystals. The cocrystal crystallizes in the $P\bar{1}$ space group with the asymmetric unit consisting of one molecule of each **dnba** and **fa**. Rotational disorder is present within the trifluoro group on the **fa** molecules. Hydrogen bonding exists between the carboxylic acids of both **dnba** and **fa**, which give the $R_2^2(8)$ ring dimer. The Hirshfeld surface of the **dnba + fa** cocrystal reveals more types of interactions. Red spots of various sizes appear on the

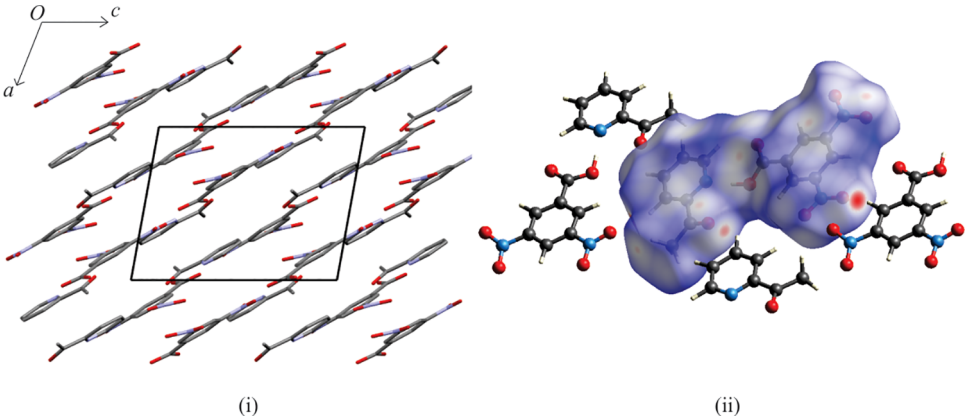

Figure 2. Crystal structure of the solvate **dnba + 2acp** showing (i) the packing (with hydrogen atoms omitted) and (ii) the d_{norm} showing some of the C−H···O interactions (surface mapped between −0.2267 and +1.0880 Å).

https://dx.doi.org/10.1021/acs.cgd.0c01217
Cryst. Growth Des. XXXX, XXX, XXX−XXX

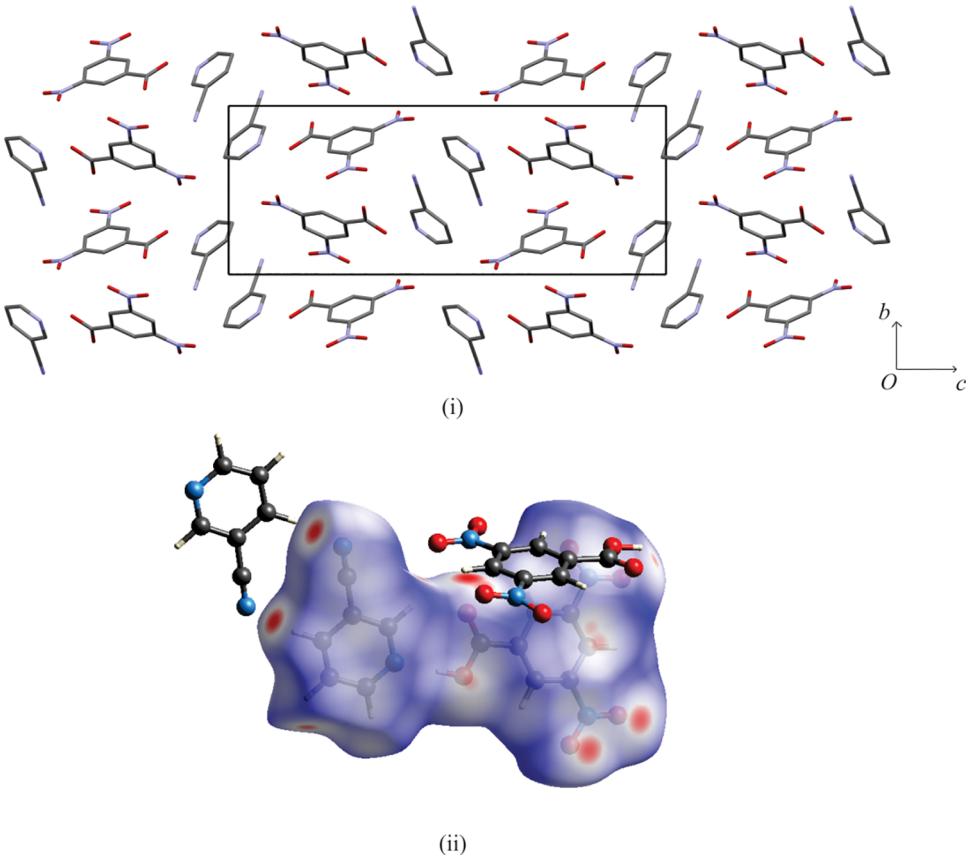

Figure 3. Crystal structure of **dnba** + **3cnp** showing (i) the packing of (with hydrogen atoms omitted) and (ii) the d_{norm} of **dnba** + **3cnp** showing the **3cnp** dimer as well as the π-hole interaction between the carboxylic acid group and one of the nitro groups (surface mapped from −0.1939 to +1.1896 Å).

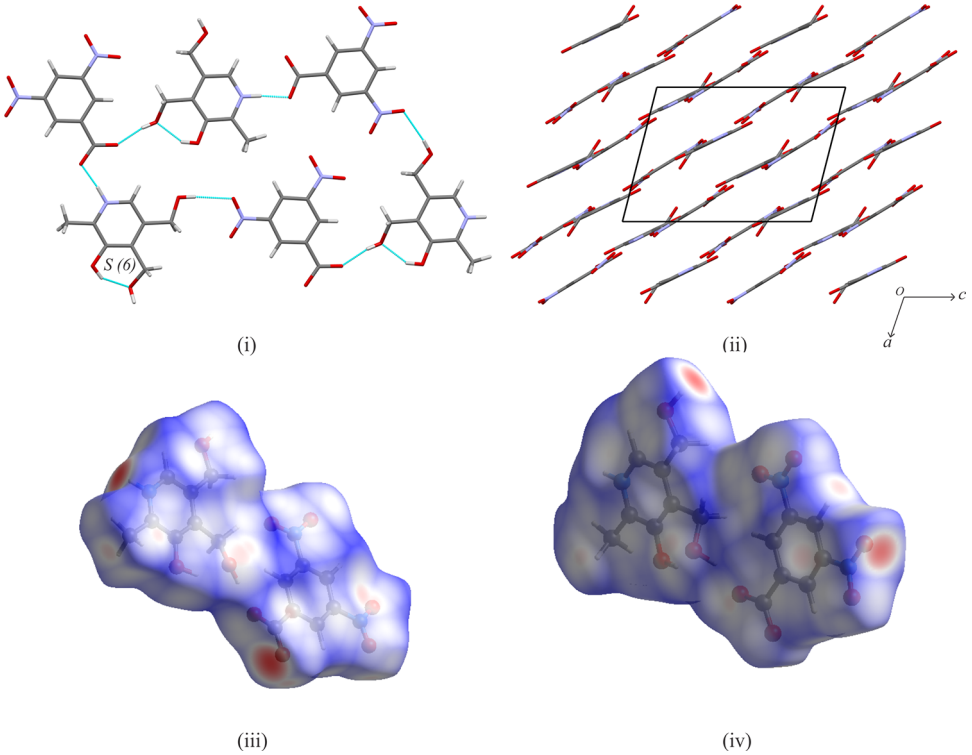

Figure 4. Crystal structure of **dnba** + **pyd** showing (i) the hydrogen bonding and (ii) the packing (with hydrogen atoms omitted) and (iii, iv) the d_{norm} from two different perspectives, where the brightest red spots are due to hydrogen bonding.

https://dx.doi.org/10.1021/acs.cgd.0c01217
Cryst. Growth Des. XXXX, XXX, XXX−XXX

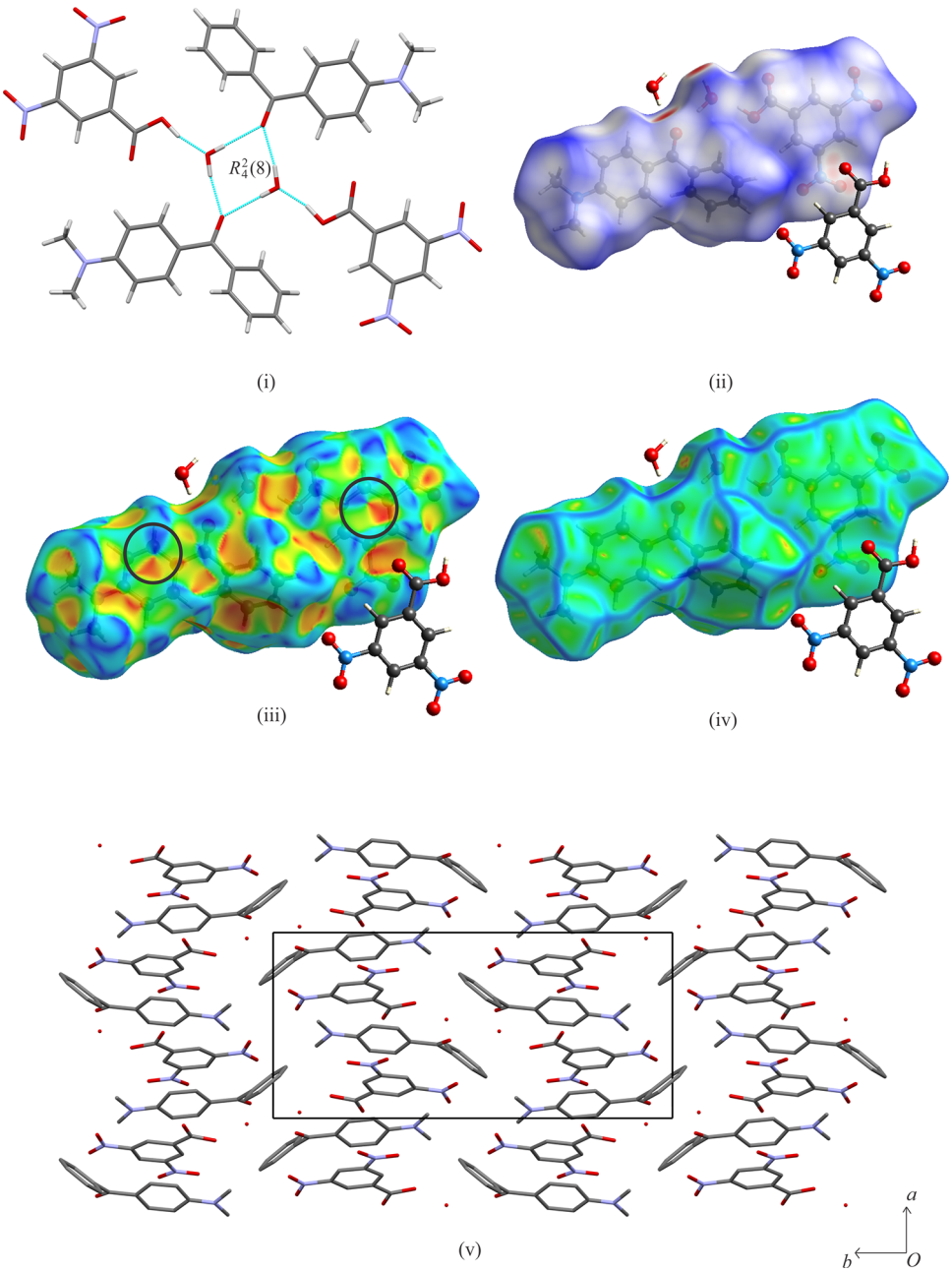

Figure 5. Crystal structure of **dnba** + **dmabp** showing (i) the hydrogen-bonded "water ring", (ii) the d_{norm} showing the π-hole interactions (mapped from −0.5738 to +1.4262 Å), (iii) the shape index with circles showing possible $\pi-\pi$ interactions, (iv) curvedness showing flat regions that could possibly allow for $\pi-\pi$ interactions, and (v) the packing diagram (with hydrogens omitted).

d_{norm}, which indicates the presence of various weak C−H···O, C−H···π, C−O···π and N−O···π interactions. Figure 6(ii) shows where some of these weak interactions may be occurring. The shape index indicates the possibility of $\pi-\pi$ stacking interactions, as indicated by the red and blue triangles in Figure 6(iii) and the presence of a flat region in the curvedness which could allow for such an interaction to exist. This $\pi-\pi$ stacking occurs between inverted dimers: i.e., between **dnba** and the benzoic acid portion of **fa**. This would lead to a layered-type packing in the structure, with the trifluorotoluene portion of **fa** separating different layers.

dnba + ***thp***. **dnba** formed a cocrystal with **thp**, which crystallized as colorless blocks (Figure 7). The asymmetric unit consists of one molecule of each **dnba** and **thp**, crystallizing in the $C2/c$ space group. The hydrogen H1 was placed geometrically with respect to O1, since this hydrogen could not be found accurately in the Fourier map. **dnba** forms a discrete hydrogen bond between the carboxylic acid O1−H1 to nitrogen N3 of **thp**. **thp** forms part of a dimer held together by two molecules of **thp** forming a ring between N4−H8···O8, with a ring graph set of $R_2^2(10)$. The overall packing is made up of several rows and columns of alternating **dnba** and **thp** molecules.

The Hirshfeld surface shows an additional set of important interactions. The brighter red spots that appear on the d_{norm} surface correspond to the stronger hydrogen bonds described previously, while the less bright spots represent weaker C−H hydrogen bonds. In addition to the strong hydrogen bond

https://dx.doi.org/10.1021/acs.cgd.0c01217
Cryst. Growth Des. XXXX, XXX, XXX−XXX

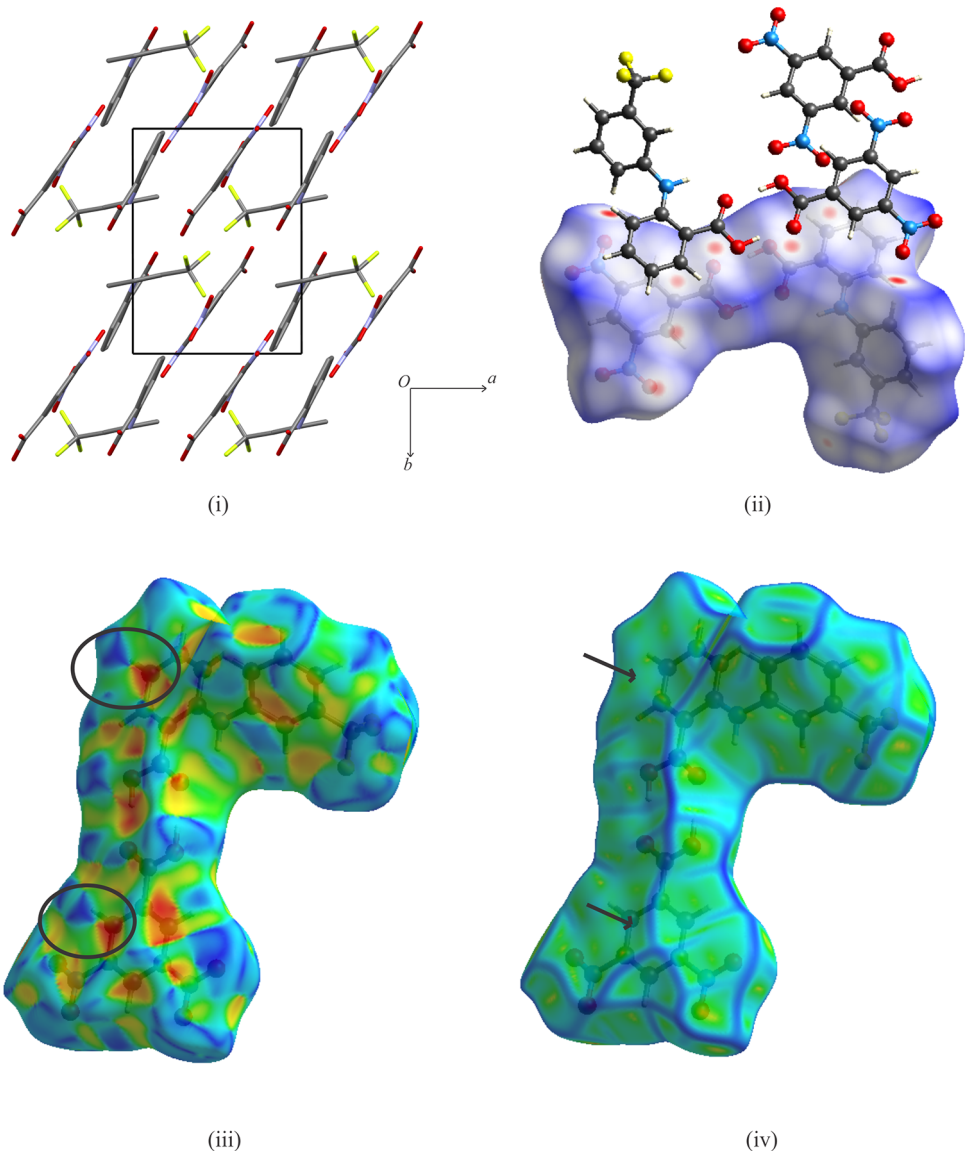

Figure 6. Crystal structure of **dnba** + **fa** showing (i) the packing (with hydrogen atoms omitted), (ii) the d_{norm} showing some of the weaker interactions present (mapped from 0.1410 to 1.4528 Å), (iii) the shape index with circles indicating the presence of some $\pi-\pi$ stacking, and (iv) the curvedness with arrows showing some flat regions where $\pi-\pi$ stacking may be possible.

between **dnba** and **thp** described previously, the weak hydrogen bond C8−H8···O2 forms. In addition, weaker hydrogen bonds form between different neighboring **dnba** molecules via C2−H2···O6 and C4−H4···O2. The presence of red and blue triangles on the shape index on both the ring of **dnba** and imidazole portion of **thp**, as well as the curvedness being flat over the aforementioned regions, indicates the presence of $\pi\cdots\pi$ stacking, which would dominate the overall packing observed in this cocrystal.

***dnba* + *tu*.** **dnba** formed a cocrystal with **tu** and crystallized as pale yellow blocks (Figure 8). This cocrystal crystallizes in the $P2_1/c$ group with the asymmetric unit consisting of one molecule each of **dnba** and **tu**. Both **dnba** and **tu** form a $R_2^2(8)$ homosynthon, which forms a set of two dimers. These dimers interact with each other via the amino group (the group not involved in the homodimer) and one of the nitro groups. In addition, a bifurcated hydrogen-bonded system arises between two **tu** molecules related to each other via the 2-fold screw axis through N4−H4A···S1 and N3−H3B···S1. The Hirshfeld surfaces indicate a π-hole-type interaction in the d_{norm} with the nitro group O3−N1−O4 interacting with the carboxylic acid group of a nearby **dnba** molecule. The packing of this cocrystal is made up of rows of **dnba** molecules alternating with channels of **tu** molecules.

Cambridge Structural Database Analysis. The analysis of the CSD indicates several trends in previously reported multicomponent crystal structures involving **dnba**. The search result of the combined query yielded 362 results. After salts containing alkali or alkakine-earth cations, heavily disordered molecules, and solvates were removed, 259 multicomponent crystal structures were examined further. Some notable examples are given in Table 5. A total of 186 of these results were binary and 73 were ternary or greater. A total of 131 entries consisted of the protonated (carboxylic acid) form, and 186 entries consisted of the deprotonated (carboxylate) form. At least 25 hydrates were reported. Only 5 entries show the formation of the carboxylic acid heterodimer $R_2^2(8)$ ring motif

https://dx.doi.org/10.1021/acs.cgd.0c01217
Cryst. Growth Des. XXXX, XXX, XXX−XXX

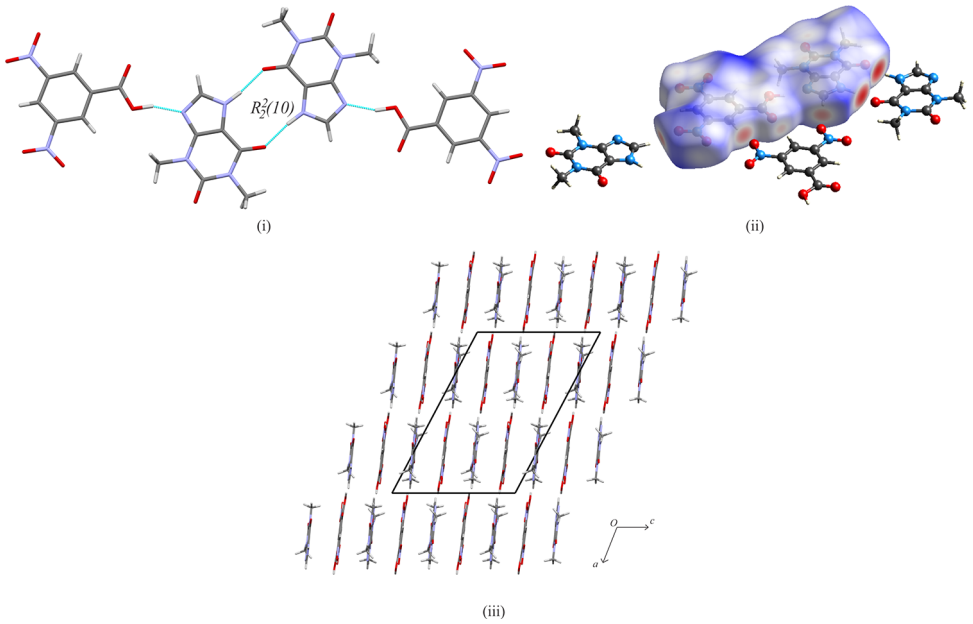

Figure 7. Crystal structure of **dnba** + **thp** showing (i) the hydrogen bonding, (ii), the d_{norm} showing some of the additional weaker hydrogen bonds (mapped from −0.5738−1.4262 Å), and (iii) the packing.

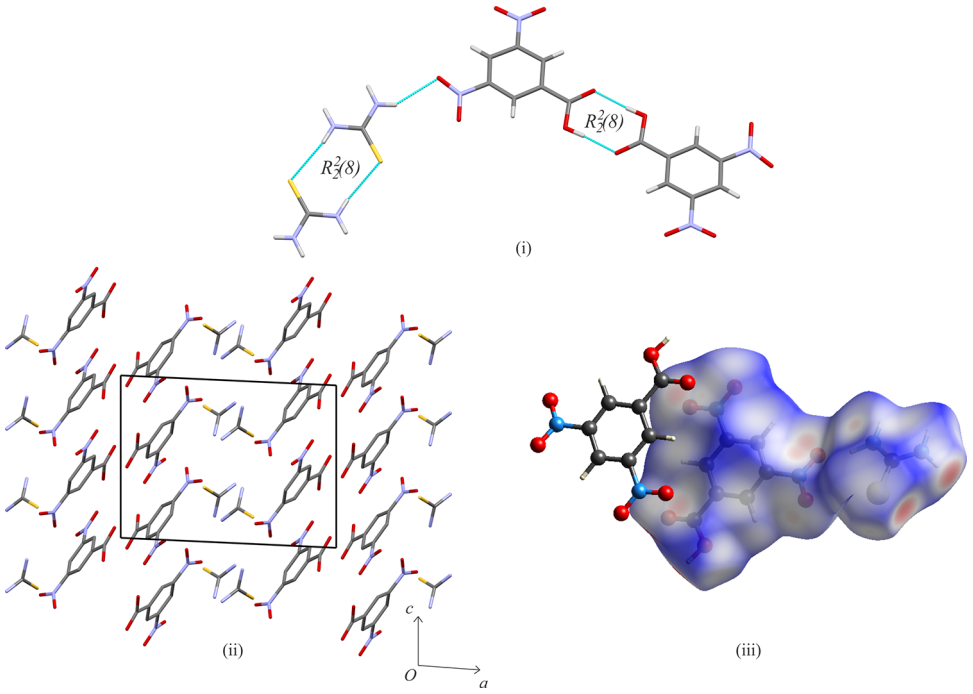

Figure 8. Crystal structure of **dnba** + **tu** showing (i) the hydrogen bonding, (ii) the packing (with hydrogen atoms omitted), and (iii) the d_{norm} showing the π-hole interaction between the nitro group and carboxylic acid (mapped from −0.7297 to +1.5105 Å).

such as that observed for the **dnba** + **fa** crystal structure, which makes the formation of this heterodimer rather rare.

One of the most common features of previously reported structures are that many coformers contain a nitrogen atom that can either act as a hydrogen bond acceptor or accepts a proton as a base and becomes ionized. Out of the total number of N-containing coformers, 66 entries include a N-containing compound that acts as a hydrogen bond acceptor (no proton transfer) and 140 consist of a proton transfer occurring from **dnba** to the N-containing compound. This result is reasonable, since **dnba** is relatively more acidic than benzoic acid (pK_a = 4.20), which will more likely result in the formation of a salt than of a cocrystal. Although most of the multicomponent crystals consisting of N-containing coformers presented in this work resulted in a cocrystal, it should be noted the multicomponent crystals present here are more an exception, rather than a part of the norm.

From Figures 2, 4, 7, and to some extent Figure 6 it seems that **dnba** tends to favor forming a layered-type structure. From the CSD, multicomponent structures which contain coformers that are relatively planar tend to favor forming a layered-type structure. This is not an absolute trend: for

https://dx.doi.org/10.1021/acs.cgd.0c01217
Cryst. Growth Des. XXXX, XXX, XXX−XXX

Table 5. Some Notable Examples of Multicomponent Crystals of dnba Presented in Other Work

refcode	comment
COLKUL	another benzoic acid derivative forming a carboxylic acid ring motif $R_2^2(8)$; also a hydrate
RAVLIM	cocrystal formed between **dnba** and 4-pyridinecarboxaldehyde; has π-hole interactions; crystals are elastic[29]
XILTAO	hydrate consisting of the carboxylate of **dnba** and 3-aminopyridinium
GAUTAM	cocrystal consisting of 4-dimethylaminobenzoic acid and **dnba**; consists of two homodimers
GOBJUQ	cocrystal consisting of **dnba** and indole-2-carboxylic acid; forms a heterodimer; layered structure
HORWIX	cocrystal consisting of carbamazepine and **dnba**; forms a heterodimer while a nitro group forms a hydrogen bond to amide not involved with the ring synthon
IDUNUQ	molecular salt formed from the proton transfer of **dnba** to 3-hydroxypyridine; carboxylate forms a hydrogen bond between the hydroxyl group and pyridyl nitrogen on two independent 3-hydroxypyridine groups
KIZQJT, KIZQOZ, KIZQUF, KIZREQ	series of charge transfer complexes formed between **dnba** and various N-substituted carbazoles; **dnba** formed a homodimer
NEMSUT	cocrystal formed between the interaction of **dnba** and phenylurea; **dnba** forms a ring synthon $R_2^2(8)$ between the carboxylic acid and amide group; remaining N−H groups form hydrogen bonds to nitro group
XAMHAX	molecular salt of **dnba** and benzimidazole; salt forms hydrogen bonds with nitro group over carboxylate

Scheme 2. Theoretical Ring Hydrogen Bond Motif between dnba and thp

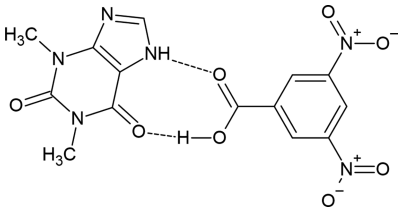

example, in the hydrate consisting of **dnba** and 4-aminosalicylic acid (refcode COLKUL) the coformers may be described as being relatively planar but the resulting structure was not simply layered.

Out of the 259 structures examined for this work, only 57 entries exhibit a hydrogen bond formed with the nitro group. In most cases, the carboxylic acid group of **dnba** dominates as the major interaction with the coformer, as observed in multicomponent crystal structures containing N-containing heterocycles. Even in cases where multiple hydrogen bond donors are available, it is not guaranteed that a hydrogen bond to the nitro group will form. It is probable that the formation of the π-hole interaction, together with other weaker interactions, is more favorable than forming a hydrogen bond with the nitro group.

For the cocrystal of **dnba** + **thp**, it should be noted that **dnba** could have formed a heterodimer, with ring synthon $R_2^2(9)$ as shown in Scheme 2. This type of heterodimer is common with cocrystals consisting of **thp** and a benzoic acid derivative, such as that occurring between **thp** and 4-aminobenzoic acid (refcode HUMNEK). However, the **thp** homodimer that was observed in **dnba** + **thp** is also common in other cocrystals involving **dnba** and a benzoic acid derivative, such as the **thp** + salicylic acid cocrystal (refcode KIGLES). The layered type structure appears to also be a common means of packing for such cocrystal systems, although exceptions do arise.

Hirshfeld Surface Analysis of dnba Complexes. It would be of interest to compare the contact contribution of **dnba** between the different multicomponent crystals presented. The percentages of the contributions from different interacting pairs is calculated by first calculating the Hirshfeld surface of **dnba** by itself and then using the values obtained from the fingerprint plots to plot a bar graph as presented in Figure 9. From Figure 9 the largest contribution comes from the O−H/H−O set of contacts, which naturally comes from the main contributing hydrogen bonds formed between **dnba**

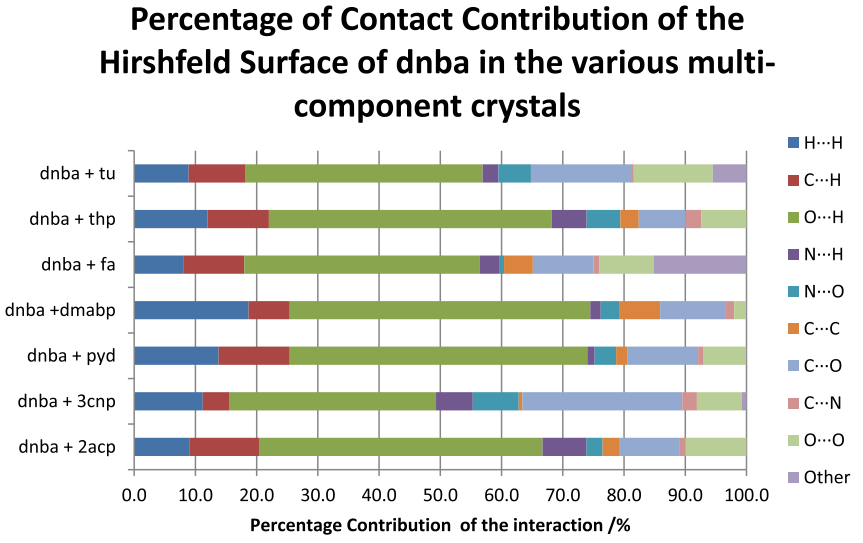

Figure 9. Percentage contribution of contacts due to **dnba**. For the cocrystal of **dnba** + **fa** the percentage contributions of F···H and O···F in other are 8.5% and 5.8%, respectively.

https://dx.doi.org/10.1021/acs.cgd.0c01217
Cryst. Growth Des. XXXX, XXX, XXX−XXX

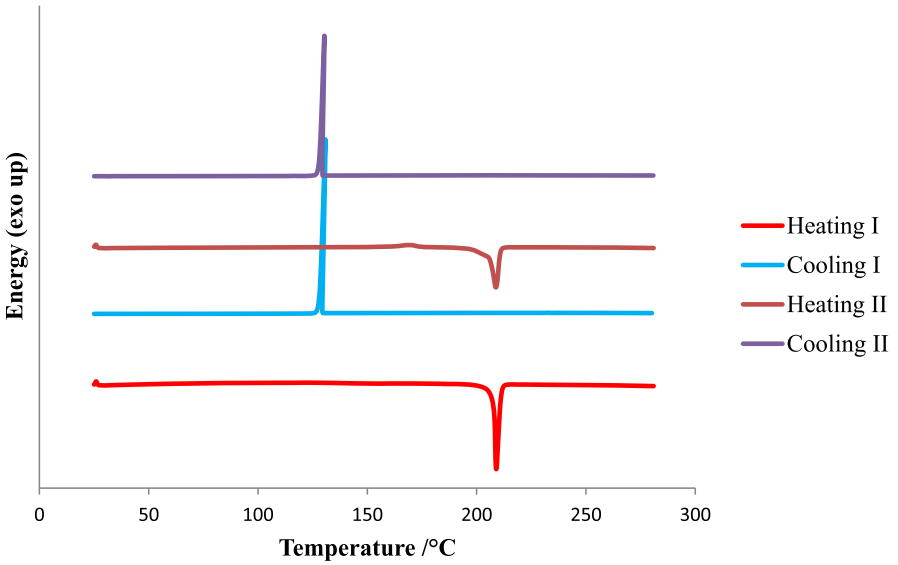

Figure 10. DSC curves for **dnba** + **2-acp**.

Table 6. Thermodynamic Data for the Melting of the Multicomponent Crystals of dnba

cocrystal/molecular salt	onset (°C)	peak (°C)	heat of fusion ΔH_{fus} (kJ mol^{-1})
dnba + **thp**	194.2	203.9	128.5
dnba + **pyd**	161.6	168.5	70.4
dnba + **2acp** (solvate)	76.8	80.9	96.4
dnba + **3cnp**	134.4	135.6	204.3
dnba + **dmabp** hydrate	86.8	93.0	91.8
dnba + **fa**	136.8	141.0	111.2
dnba + **tu**	153.2	156.3	179.5

and its respective coformer(s). Other notable sets of contacts include C···H and C···O. The C···O set of contacts contributes to a large percentage toward the total, especially for the **dnba** + **3cnp**. These arise due to the π-hole-type interactions present across the various multicomponent crystals. The C···H contacts arise due to the C−H···π, and its significance has been noted before. The percentage of C−C contacts in the cocrystal of **dnba** + **fa** and the hydrate of **dnba** + **dmabp** is much higher than the rest due to the presence of $\pi-\pi$ stacking interactions. Overall the contact contributions of the different contacts across the different multicomponents are similar to each other to an extent.

Differential Scanning Calorimetry. Differential scanning calorimetry was carried out on all samples. In each case, the sample was heated to 250 °C and then cooled to 40 °C twice at a heating/cooling rate of 10 °C/min under ambient conditions. In each case only one thermal event was observed—the melting peak with no recrystallization. The exceptions to this are the cocrystals of **dnba** + **thp** and **dnba** + **3cnp** and the solvate **dnba** + **2acp**. In these crystal systems, upon cooling back to 25 °C, a peak corresponding to recrystallization is observed. Upon heating and cooling a second time, the same peaks are observed, indicating a degree of reversibility. The DSC curves for the heating and cooling of **dnba** + **2acp** are represented in Figure 10, as an example of the thermal behavior observed for **dnba** + **thp** and **dnba** + **2acp**. The rest of the DSC curves are available in the Supporting Information. Table 6 contains the thermodynamic behavior related to the melting of each of the multicomponent crystals.

CONCLUSIONS

Seven multicomponent crystals, of which five are cocrystals, one is a solvate, and one is a molecular salt, consisting of **dnba** were synthesized and characterized. These crystals showed various hydrogen-bonding interactions between **dnba** and the coformer. Hirshfeld surfaces show that a number of weaker interactions exist within each crystal, which contributes to the overall structure and packing of the molecules in the crystals. For future work, it would be of use to determine if the cocrystals of **dnba** + **thp** and **dnba** + **fa** have any improved properties such as solubility over the parent API molecule. Overall, this work shows that **dnba** can be a versatile molecule to consider in the development of new multicomponent crystals involving APIs.

ASSOCIATED CONTENT

Supporting Information

The Supporting Information is available free of charge at https://pubs.acs.org/doi/10.1021/acs.cgd.0c01217.

Powder X-ray diffraction data, differential scanning calorimetry data, and the Hirshfeld surface diagrams and fingerprint plots (PDF)

Accession Codes

CCDC 2026651−2026657 contain the supplementary crystallographic data for this paper. These data can be obtained free of charge via www.ccdc.cam.ac.uk/data_request/cif, or by emailing data_request@ccdc.cam.ac.uk, or by contacting The Cambridge Crystallographic Data Centre, 12 Union Road, Cambridge CB2 1EZ, UK; fax: +44 1223 336033.

AUTHOR INFORMATION

Corresponding Author

Andreas Lemmerer − *Molecular Sciences Institute, School of Chemistry, University of the Witwatersrand, 2050 Johannesburg, South Africa;* orcid.org/0000-0003-1569-2831; Phone: +27-11-717-6711;

https://dx.doi.org/10.1021/acs.cgd.0c01217
Cryst. Growth Des. XXXX, XXX, XXX−XXX

Email: andreas.lemmerer@wits.ac.za; Fax: +27-11-717-6749

Author

Matthew C. Scheepers − *Molecular Sciences Institute, School of Chemistry, University of the Witwatersrand, 2050 Johannesburg, South Africa*

Complete contact information is available at: https://pubs.acs.org/10.1021/acs.cgd.0c01217

Notes

The authors declare no competing financial interest.

■ ACKNOWLEDGMENTS

We acknowledge and thank the DSI/NRF Centre of Excellence in Strong Materials as well as the NRF for funding the Bruker D2 Phaser diffractometer.

■ REFERENCES

(1) Vishweshwar, P.; McMahon, J. A.; Bis, J. A.; Zaworotko, M. J. Pharmaceutical Co-Crystals. *J. Pharm. Sci.* **2006**, *95*, 499−516.
(2) Schultheiss, N.; Newman, A. Pharmaceutical Cocrystals and Their Physicochemical Properties. *Cryst. Growth Des.* **2009**, *9*, 2950−2967.
(3) Karimi-Jafari, M.; Padrela, L.; Walker, G. M.; Croker, D. M. Creating Cocrystals: A review of Pharmaceutical Cocrystal Preparation Routes and Applications. *Cryst. Growth Des.* **2018**, *18*, 6370−6387.
(4) Zhou, Z.; Li, W.; Sun, W. J.; Lu, T.; Tong, H. H. Y.; Sun, C. C.; Zheng, Y. Resveratrol cocrystals with enhanced solubility and tabletability. *Int. J. Pharm.* **2016**, *509*, 391−399.
(5) Stanton, M. K.; Kelly, R. C.; Colletti, A.; Kiang, Y. H.; Langley, M.; Munson, E. J.; Peterson, M. L.; Roberts, J.; Wells, M. Improved Pharmacokinetics of AMG 517 Through Co-Crystallization Part 1: Comparison of Two Acids With Corresponding Amide Co-crystals. *J. Pharm. Sci.* **2010**, *99*, 3769−3778.
(6) Groom, C. R.; Bruno, I. J.; Lightfoot, M. P.; Ward, S. C. The Cambridge Structural Database. *Acta Crystallogr., Sect. B: Struct. Sci., Cryst. Eng. Mater.* **2016**, *72*, 171−179.
(7) Shaibah, M. A. E; Yathirajan, H. S.; Rathore, R. S.; Furuya, T.; Haraguchi, T.; Akitsu, T.; Glidewell, C. Co-crystallization of 3,5-dinitrobenzoic acid with two antipsychotic agents: a simple 1:1 salt with trihexyphenidyl and a 1:2 acid salt containing a very short O—H···O hydrogen bond with chlorprothixene. *Acta Cryst. Sect. E* **2019**, *75*, 292−298.
(8) Aitipamula, S.; Chow, P. S.; Tan, R. B. H. Polymorphs and Solvates of a Cocrystal Involving an Analgesic Drug, Ethenzamide, and 3,5-Dinitrobenzoic Acid. *Cryst. Growth Des.* **2010**, *10*, 2229−2238.
(9) Pawlędzio, S.; Trzybiński, D.; Woźniak, K. Crystal structure and energetic features of the cocrystal of carbamazepine with 3,5-dinitrobenzoic acid. *Acta Crystallogr., Sect. C: Struct. Chem.* **2019**, *75*, 1150−1156.
(10) Liu, X.; Su, Z.; Ji, W.; Chen, S.; Wei, Q.; Xie, G.; Yang, X.; Gao, S. Structure, Physicochemical Properties, and Density Functional Theory Calculation of High-Energy-Density Materials Constructed with Intermolecular Interaction: Nitro Group Charge Determines Sensitivity. *J. Phys. Chem. C* **2014**, *118*, 23487−23498.
(11) Hill, T. N.; Levendis, D. C.; Lemmerer, A. Binary and ternary co-crystals and molecular salts of 3,5-dinitrobenzoic acid: A many-faceted supramolecular reagent. *J. Mol. Struct.* **2018**, *1168*, 28−38.
(12) Ford, S. J.; McIntyre, G. J.; Johnson, M. R.; Evans, I. R. Structure and dynamics studies of the short strong hydrogen bond in the 3,5-dinitrobenzoic acid−nicotinic acid molecular complex. *CrystEngComm* **2013**, *15*, 7576−7582.
(13) Tothadi, S.; Desiraju, G. R. Unusual co-crystal of isonicotinamide: the structural landscape in crystal engineering. *Philos. Trans. R. Soc., A* **2012**, *370*, 2900−2915.
(14) Santiago de Oliveira, Y.; Saraiva Costa, W.; Ferreira Borges, P.; Silmara Alves de Santana, M.; Ayala, A. P. The design of novel metronidazole benzoate structures: exploring stoichiometric diversity. *Acta Crystallogr., Sect. C: Struct. Chem.* **2019**, *75*, 483−495.
(15) Girisha, M.; Yathirajan, H. S.; Jasinski, J. P.; Glidewell, C. Different acid−base behaviour of a pyrazole and an isoxazole with organic acids: crystal and molecular structures of the salt 3-(4-fluorophenyl)-1H-pyrazolium 2,4,6-trinitrophenolate and of the cocrystal 4-amino-N-(3,4-dimethyl-1,2-oxazol-5-yl)-benzenesulfonamide−3,5-dinitrobenzoic acid (1/1). *Acta Crystallogr., Sect. C: Struct. Chem.* **2016**, *72*, 612−618.
(16) Bauzá, A.; Mooibroek, T. J.; Frontera, A. Directionality of π-holes in nitro compounds. *Chem. Commun.* **2015**, *51*, 1491−1493.
(17) Ebisuzaki, Y.; Boyle, P. D.; Smith, J. A. Methylxanthines. I. Anhydrous Theophylline. *Acta Crystallogr., Sect. C: Cryst. Struct. Commun.* **1997**, *53*, 777−779.
(18) Rossi, F.; Cerreia Vioglio, P.; Bordignon, S.; Giorgio, V.; Nervi, C.; Priola, E.; Gobetto, R.; Yazawa, K.; Chierotti, M. R. Unraveling the Hydrogen Bond Network in a Theophylline−Pyridoxine Salt Cocrystal by a Combined X-ray Diffraction, Solid-State NMR, and Computational Approach. *Cryst. Growth Des.* **2018**, *18*, 2225−2233.
(19) Van Hoeck, E.; De Schaetzen, T.; Pacquet, C.; Bolle, F.; Boxus, L.; Van Loco, J. Analysis of benzophenone and 4-methylbenzophenone in breakfast cereals using ultrasonic extraction in combination with gas chromatography−tandem mass spectrometry (GC−MS n). *Anal. Chim. Acta* **2010**, *663*, 55−59.
(20) *Bruker, SAINT+, ver. 6.02 (including XPREP)*, Bruker AXS Inc.: Madison, WI, USA, 1999. Cruz-Cabeza, A. J. Acid−base crystalline complexes and the pK_a rule. *CrystEngComm.* **2012**, *14*, 6362−6365.
(21) Sheldrick, G. M.; *SHELX, release 97-2 (includes SHELXS and SHELXL)*; University of Göttingen: 1997.
(22) Farrugia, L. J. ORTEP-3 for Windows - a version of ORTEP-III with a Graphical User Interface (GUI). *J. Appl. Crystallogr.* **1997**, *30*, 565−565.
(23) Macrae, C. F.; Edgington, P. R.; McCabe, P.; Pidcock, E.; Shields, G. P.; Taylor, R.; Towler, M.; van de Streek, J. Mercury: visualization and analysis of crystal structures. *J. Appl. Crystallogr.* **2006**, *39*, 453−457.
(24) Spackman, M. A.; McKinnon, J. J. Hirshfeld surface analysis. *CrystEngComm* **2002**, *4*, 378−392.
(25) McKinnon, J. J.; Spackman, M. A.; Mitchell, A. S. Novel tools for visualizing and exploring intermolecular interactions in molecular crystals. *Acta Crystallogr., Sect. B: Struct. Sci.* **2004**, *60*, 627−668.
(26) Turner, M. J.; McKinnon, J. J.; Wolff, S. K.; Grimwood, D. J.; Spackman, P. R.; Jayatilaka, D.; Spackman, M. A.; *CrystalExplorer 17.5*; The University of Western Australia: 2017.
(27) Cruz-Cabeza, A. J. Acid−base crystalline complexes and the pKa rule. *CrystEngComm* **2012**, *14*, 6362−6365.
(28) SciFinder: https://scifinder.cas.org/scifinder/view/scifinder/scifinderExplore.jsf. Date of Access: September 19−22, 2018.
(29) Saha, S.; Desiraju, G. R. σ-Hole and π-Hole Synthon Mimicry in Third-Generation Crystal Engineering: Design of Elastic Crystals. *Chem. - Eur. J.* **2017**, *23*, 4936−4943.

https://dx.doi.org/10.1021/acs.cgd.0c01217
Cryst. Growth Des. XXXX, XXX, XXX−XXX